Contents lists available at ScienceDirect

Nuclear Engineering and Technology

journal homepage: www.elsevier.com/locate/net

Original Article

Numerical analysis of the electromagnetic force for design optimization of a rectangular direct current electromagnetic pump

Geun Hyeong Lee, Hee Reyoung Kim[*]

Department of Nuclear Engineering, Ulsan National Institute of Science and Technology, Ulsan 689-798, Republic of Korea

A B S T R A C T

The force of a direct current (DC) electromagnetic pump used to transport liquid lithium was analyzed to optimize its geometrical and electrical parameters by numerical simulation. In a heavy-ion accelerator, which is being developed in Korea, a liquid lithium film is utilized for its high charge-stripping efficiency for heavy ions of uranium. A DC electromagnetic pump with a flow rate of 6 cm^3/s and a developed pressure of 1.5 MPa at a temperature of 200°C was required to circulate the liquid lithium to form liquid lithium films. The current and magnetic flux densities in the flow gap, where a Sm_2Co_{17} permanent magnet was used to generate a magnetic field, were analyzed for the electromagnetic force distribution generated in the pump. The pressure developed by the Lorentz force on the electromagnetic force was calculated by considering the electromotive force and hydraulic pressure drop in the narrow flow channel. The opposite force at the end part due to the magnetic flux density in the opposite direction depended on the pump geometrical parameters such as the pump duct length and width that defines the rectangular channels in the nonhomogeneous distributions of the current and magnetic fields.

1. Introduction

Electromagnetic pumps are employed to circulate liquid metals with high electrical conductivity using the Lorentz force whose value is calculated as the cross product of the current and the magnetic field perpendicular to it [1,2]. The heavy-ion accelerator, which is being developed in Korea, uses a liquid lithium film as a charge stripper [3] to increase the acceleration efficiency of uranium heavy ions. The uranium ions with a charge of 33+ become uranium ions with a charge of 78+, which pass through a liquid lithium film with a thickness of less than 25 μm. The direct current (DC) electromagnetic pump causes the liquid lithium to circulate to generate thin liquid lithium films from a high-speed jet of 60 m/s at the injection nozzle of the charge-stripper system, which is subjected to a high hydraulic pressure loss at a low flow rate [4].

In the present study, the distributions of the current [5] and magnetic flux densities in the narrow channel of such pump with a finite-length permanent magnet were analyzed [6]. The developed pressure, which depends on the Lorentz force and hydraulic pressure drop, was analyzed by numerical simulation using the ANSYS code. Analyses were performed on the changes in the geometrical and electrical parameters by considering the distributions of the current and magnetic flux densities for the required pressure and flow rate [7]. The geometrical and electromagnetic parameters of the pump were optimized to satisfy the requirement of a developed pressure of 1.5 MPa and flow rate of 6 cm^3/s under an operating temperature of 200°C.

2. Mathematical setup for analysis

The DC electromagnetic pump was divided into three parts, namely an electrode stub that transports current to the liquid metal, permanent magnets with a thickness of 50 mm to generate the magnetic flux for the liquid metal, and a 1-mm-thick pump duct [8], as shown in Fig. 1. The electrode stub and permanent magnets are arranged in the x and z directions, respectively, by applying the Cartesian coordinate system to the rectangular pump shown in Fig. 1 [9,10]. Liquid lithium flows along the y direction because of the developed pressure from the Lorentz force, which was generated by the vector product of the current through the electrode stub in the x direction and the magnetic field B from the permanent magnets in the z direction [11]. The governing equations, which consist of magnetohydrodynamic equations, to solve the force generated in the DC electromagnetic pump are expressed in Equations (1)–(5). This set of equations was solved using the ANSYS code to determine the magnetic field and current density. The Maxwell equations were applied to solve the induced magnetic

* Corresponding author.
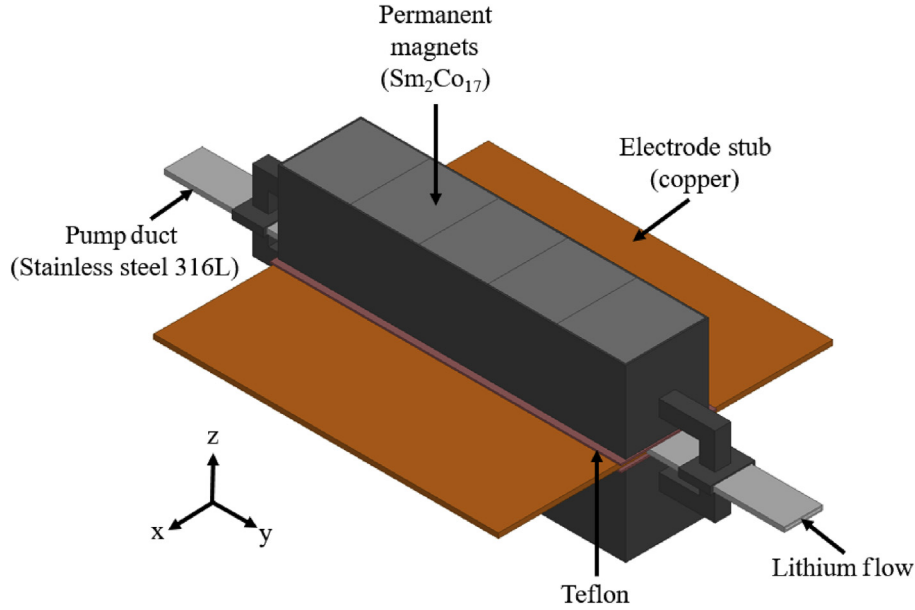E-mail address: kimhr@unist.ac.kr (H.R. Kim).

Fig. 1. Schematic of the DC electromagnetic pump.
DC, direct current.

flux density, and Ohm's law was used to calculate the current density. The force and pressure drop of the DC electromagnetic pump were calculated using the Navier–Stokes equation, where the electromagnetic force $J \times B$ was added to the last term in Equation (5) as an external force [12].

Ampere's law: $\nabla \times \overrightarrow{B} = \mu_0 \left(\overrightarrow{J} + \varepsilon_0 \dfrac{\partial E}{\partial t} \right)$ (1)

Faraday's law: $\nabla \times \overrightarrow{E} = -\dfrac{\partial \overrightarrow{B}}{\partial t}$ (2)

Gauss's law for magnetism: $\nabla \cdot \overrightarrow{B} = 0$ (3)

Ohm's law : $\overrightarrow{J} = \sigma \left(\overrightarrow{E} + \overrightarrow{v} \times \overrightarrow{B} \right)$ (4)

Navier − Stokes equation : $\dfrac{\partial \overrightarrow{v}}{\partial t} + (\overrightarrow{v} \cdot \nabla) \overrightarrow{v}$
$$= -\frac{1}{\rho} \nabla \left(\overrightarrow{p} + \overrightarrow{p_h} \right) + \nu \nabla^2 \overrightarrow{v} + \frac{1}{\rho} \overrightarrow{J_t} \times \overrightarrow{B}$$ (5)

The components of the electric field, current density, magnetic flux density, and velocity of fluid are expressed in Equations (6)–(11) according to the Cartesian coordinate system. The z-direction electric field of the DC electromagnetic pump was disregarded because of the nonconductive material (Teflon) between the permanent magnet and pump duct to avoid a z-direction current from flowing to the permanent magnet and narrow the gap of the flow channel, as expressed in Equation (6). The permanent magnet creates a magnetic field because of its rotating electrons. The microscopically small circulating current in the permanent magnet was negligible in the analysis of the induced current. Therefore, the magnetic flux density was divided into an external magnetic flux density from the permanent magnet and the induced magnetic flux density from the current density to avoid confusion in the magnitude of the induced magnetic flux density according to Equation (8). The fluid velocity was only taken along the y direction

owing to the laminar flow at the low Reynolds number according to Equation (11).

$\overrightarrow{E}_t(x,y,z) = E_x \widehat{x} + E_y \widehat{y}$ (6)

$\overrightarrow{J}_t(x,y,z) = J_x \widehat{x} + J_y \widehat{y} + J_z \widehat{z}$ (7)

$\overrightarrow{B}_t(x,y,z) = \overrightarrow{B}_e(x,y,z) + \overrightarrow{B}_i(x,y,z)$ (8)

$\overrightarrow{B}_e(x,y,z) = B_{e,x} \widehat{x} + B_{e,y} \widehat{y} + B_{e,z} \widehat{z}$ (9)

$\overrightarrow{B}_i(x,y,z) = B_{i,x} \widehat{x} + B_{i,y} \widehat{y} + B_{i,z} \widehat{z}$ (10)

$\overrightarrow{v}(x,y,z) = v_y \widehat{y}$ (11)

Ampere's law in Equation (1) can be expressed as Equations (12)–(15) using the curl operator calculation in the Cartesian coordinate system where the time-varying electric field term was not considered because the DC electromagnetic pump used the DC source. Only the induced magnetic flux density was affected by the current density because the external magnetic flux density was affected by the small circulating current in the permanent magnet.

$\nabla \times \overrightarrow{B}_i = \mu_0 \overrightarrow{J}_t$ (12)

$\nabla \times \overrightarrow{B}_i = \left(\dfrac{\partial B_{i,z}}{\partial y} - \dfrac{\partial B_{i,y}}{\partial z} \right) \widehat{x} + \left(\dfrac{\partial B_{i,x}}{\partial z} - \dfrac{\partial B_{i,z}}{\partial x} \right) \widehat{y} + \left(\dfrac{\partial B_{i,y}}{\partial x} - \dfrac{\partial B_{i,x}}{\partial y} \right) \widehat{z}$ (13)

$\mu_0 \overrightarrow{J}_t = \mu_0 \left(J_x \widehat{x} + J_y \widehat{y} + J_z \widehat{z} \right)$ (14)

$\dfrac{\partial B_{i,z}}{\partial y} - \dfrac{\partial B_{i,y}}{\partial z} = \mu_0 J_x, \quad \dfrac{\partial B_{i,x}}{\partial z} - \dfrac{\partial B_{i,z}}{\partial x} = \mu_0 J_y, \quad \dfrac{\partial B_{i,y}}{\partial x} - \dfrac{\partial B_{i,x}}{\partial y} = \mu_0 J_z$ (15)

Faraday's law in Equation (2) can be expressed as Equations (16)–(18) using the curl operator calculation in the Cartesian coordinate system where the time-varying magnetic flux density term was neglected because of the DC source and permanent magnet.

$$\nabla \times \vec{E}_t = 0 \tag{16}$$

$$\nabla \times \vec{E}_t = -\frac{\partial E_y}{\partial z}\hat{x} + \frac{\partial E_x}{\partial z}\hat{y} + \left(\frac{\partial E_y}{\partial x} - \frac{\partial E_x}{\partial y}\right)\hat{z} \tag{17}$$

$$\frac{\partial E_y}{\partial z}\hat{x} = 0, \quad \frac{\partial E_x}{\partial z} = 0, \quad \frac{\partial E_y}{\partial x} - \frac{\partial E_x}{\partial y} = 0 \tag{18}$$

Gauss's law for magnetism in Equation (3) can be expressed using the divergence operator in the Cartesian coordinate system as Equations (19)–(22). The divergence in the external and internal magnetic flux densities became zero.

$$\nabla \cdot \vec{B}_e = 0 \tag{19}$$

$$\nabla \cdot \vec{B}_i = 0 \tag{20}$$

$$\nabla \cdot \vec{B}_e = \frac{\partial (B_{e,x})}{\partial x} + \frac{\partial (B_{e,y})}{\partial y} + \frac{\partial (B_{e,z})}{\partial z} = 0 \tag{21}$$

$$\nabla \cdot \vec{B}_i = \frac{\partial (B_{i,x})}{\partial x} + \frac{\partial (B_{i,y})}{\partial y} + \frac{\partial (B_{i,z})}{\partial z} = 0 \tag{22}$$

Ohm's law in Equation (4) can be expressed as Equations (23)–(26) using the vector product of the velocity and magnetic flux density.

$$\vec{J}_t = \sigma(\vec{E}_t + \vec{v} \times \vec{B}_t) \tag{23}$$

$$\vec{J}_t = J_x\hat{x} + J_y\hat{y} + J_z\hat{z} \tag{24}$$

$$\sigma(\vec{E}_t + \vec{v} \times \vec{B}_t) = \sigma\{(E_x + v_yB_{i,z} + v_yB_{e,z})\hat{x} + E_y\hat{y} - (v_yB_{i,x} - v_yB_{e,x})\hat{z}\} \tag{25}$$

$$J_x = \sigma(E_x + v_yB_{i,z} + v_yB_{e,z}), \; J_y = \sigma E_y, \; J_z = \sigma(v_yB_{i,x} - v_yB_{e,x}) \tag{26}$$

Therefore, the equation for the magnetic flux density is derived as Equation (27) from Equations (15), (18), (22) and (26).

$$\frac{1}{\mu_0\sigma}\left(\frac{\partial^2 B_{i,z}}{\partial y \partial z} - \frac{\partial^2 B_{i,y}}{\partial z^2}\right) = v_yB_{i,z} + v_yB_{e,z}, \; \frac{1}{\mu_0\sigma}\left(\frac{\partial^2 B_{i,z}}{\partial x \partial z} - \frac{\partial^2 B_{i,x}}{\partial z^2}\right) = 0 \tag{27}$$

The force density of the DC electromagnetic pump can be calculated using Equation (28) as the vector product of the current density in Equation (26) and magnetic flux density in Equations (8)–(10). Only the y direction of the force density is needed to develop the pressure of the DC electromagnetic pump. Therefore, the x direction of the electric field and z and x directions of the magnetic flux densities were the only considered factors. In this study, the electromotive force (EMF) is defined as a disturbed force in Equation (29), and the Lorentz force is defined as another force in Equation (30).

$$\begin{aligned}\vec{f} &= \vec{J}_t \times \vec{B}_t \\ &= \{\sigma E_y(B_{i,z} + B_{e,z}) - \sigma(v_yB_{i,x} - v_yB_{e,x})(B_{i,y} + B_{e,y})\}\hat{x} + \{\sigma(E_x \\ &\quad + v_yB_{i,z} + v_yB_{e,z})(B_{i,z} + B_{e,z}) - \sigma(v_yB_{i,x} + v_yB_{e,x})(B_{i,x} \\ &\quad + B_{e,x})\}\hat{y} + \{\sigma(E_x + v_yB_{i,z} + v_yB_{e,z})(B_{i,y} + B_{e,y}) - \sigma E_y(B_{i,x} \\ &\quad + B_{e,x})\}\hat{z}\end{aligned} \tag{28}$$

$$f_E = -\sigma(v_yB_{i,x} + v_yB_{e,x})(B_{i,x} + B_{e,x}) \tag{29}$$

$$f_L = \sigma(E_x + v_yB_{i,z} + v_yB_{e,z})(B_{i,z} + B_{e,z}) \tag{30}$$
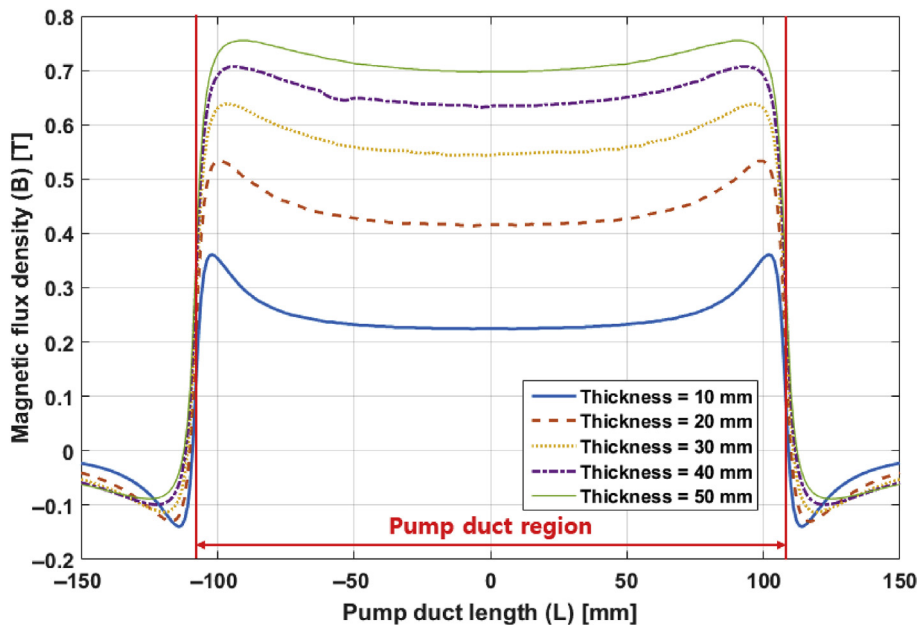

Fig. 2. Linear magnetic flux density distribution with the change in the permanent magnet thickness.

The Navier–Stokes equation is reduced to Equation (31) for the steady-state incompressible flow of liquid lithium [13], where the viscosity term was neglected because of the high Hartmann number of the electromagnetic pump. Therefore, the pressure gradient in the Navier–Stokes equation can be expressed as a force density and a hydraulic pressure loss [14].

$$\nabla p = \vec{J_t} \times \vec{B} - \nabla p_h \tag{31}$$

Hydraulic pressure loss Δp_h [15] was calculated using the Darcy–Weisbach formula in Equation (32), where the Darcy friction coefficient f_d of the laminar flow is expressed as Equation (33).

$$\Delta p_h = \frac{f_d \rho L v_z^2 (W_d + H_d)}{4 W_d H_d} \tag{32}$$

$$f_d = 64/Re \tag{33}$$

Combining Equations (28)–(32) yields the developed pressure, as expressed in Equation (34).

$$\Delta p = \int \{\sigma(E_x + v_y B_{i,z} + v_y B_{e,z})(B_{i,z} + B_{e,z}) - \sigma(v_y B_{i,x} - v_y B_{e,x})$$
$$\times (B_{i,x} + B_{e,x})\} dy - \frac{f_d \rho L v_z^2 (W_d + H_d)}{4 W_d H_d}$$
$$\tag{34}$$

Additionally, the permissible current at the electrode stub obtained by the Melson and Both equations are expressed as in Equation (35) to define the pump duct length.
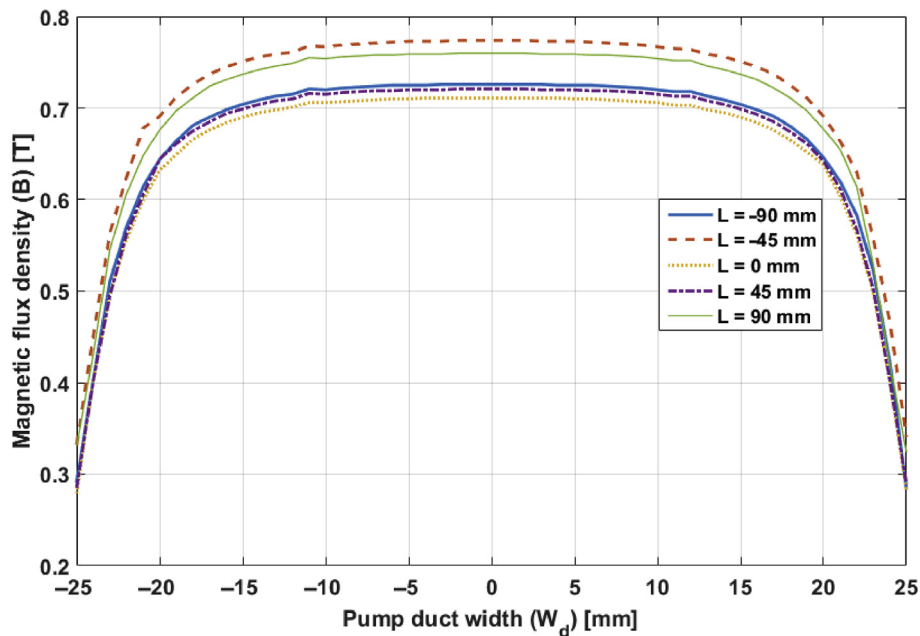

Fig. 3. Linear magnetic flux density distribution parallel to pump duct width at pump duct length $L = -20, -10, 0, 10,$ and 20 and at the midpoint of the pump duct height.
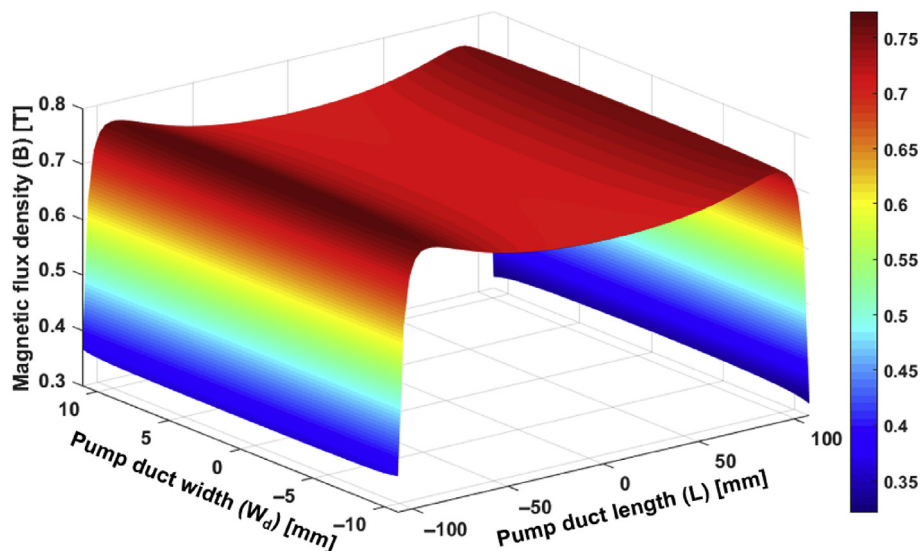

Fig. 4. Three-dimensional magnetic flux density distribution in liquid lithium at the midpoint of the pump duct height.

$$I_p = 24.9K(T - T_n)^{0.61}S^{0.5}p_e^{0.39} \Big/ \sqrt{\rho'_{|20°C}[1 + \alpha(T - 293)]} \quad (35)$$

The force density expressed in Equation (28) was solved to obtain a developed pressure of 1.5 MPa and flow rate of 6 cm³/s in Equation (34) using the finite-element method in the ANSYS code simulation with the model in Fig. 1 through the magnetic flux density owing to magnetic permeability and coercivity and current density owing to bulk conductivity [16].

3. Results and discussion

3.1. Magnetic flux density

The magnetic flux density of the Sm_2Co_{17} permanent magnet increased as the thickness of the permanent magnet increased [17], as shown in Fig. 2, where the mechanically permissible maximum thickness of the permanent magnet was 50 mm. The temperature

Table 1
Design specifications of the DC electromagnetic pump.

	Design variables	Unit	Values
Hydrodynamic	Flow rate (Q)	[m³/s]	6×10^{-6}
	Total pressure (ΔP)	[MPa]	1.5
	Temperature (T)	[K]	473
	Velocity (v)	[m/s]	0.27
	Reynolds number (R_e)		471
	Developed pressure due to Lorentz force (ΔP_L)	[MPa]	1.617
	Pressure loss due to EMF (ΔP_E)	[MPa]	0.117
	Hydraulic pressure loss (ΔP_H)	[MPa]	2.6×10^{-4}
Geometrical	Height (H_d)	[mm]	1
	Width (W_d)	[mm]	22
	Length (L)	[mm]	216
	Thickness (t_h)	[mm]	1
Electrical	Conductivity of permanent magnet	[1/(Ω·m)]	1,111,111
	Conductivity of pump duct	[1/(Ω·m)]	1,111,790
	Conductivity of liquid lithium	[1/(Ω·m)]	3,804,900
	Input current (i_t)	[A]	3740
	Voltage	[V]	0.08
	Power	[W]	253

DC, direct current; EMF, electromotive force.

of the electrode stub was fixed as the condition of lithium (200°C); therefore, the pump duct length was fixed as 216 mm, considering the permissible current as described in Equation (35). The length of the permanent magnet also fixed as 216 mm, and the width of permanent magnet was set to maximize the magnetic flux density. Fig. 3 shows that the magnetic flux density varied according to the pump duct width. The magnetic flux density in the radial direction exhibited ~99% of its maximum value when the width of the permanent magnet was between −11 and 11 mm, as shown in Fig. 3, which shows the magnetic flux density according to the pump duct width and length. Fig. 3 shows that the pump duct width should be 22 mm to maximize the generation of the Lorentz force. Fig. 4, which represents the tendency of the magnetic flux density in pump duct, shows that the magnetic flux density of the permanent magnet has a maximum value of 0.759 T and minimum value of 0.751 T at the center and edges of the pump duct width and maximum pump duct length, respectively [18]. The permanent magnets were arranged parallel to the pump duct length with maximum width and thickness, as shown in Fig. 1. The magnetic flux density was asymmetric along the length of the pump duct because it was affected by the electrical current according to Equations (15) and (26). The magnetic flux density was affected by the electric field according to Ampere's law and Ohm's law, and its direction was positive at the left side and negative at the right side.

3.2. Current density

The electrical parameters to analyze the current density of the DC electromagnetic pump are given in Table 1. The current from the DC electromagnetic pump passed from the electrode stub to the pump duct, which is made of 316L stainless steel [19], before branching to the permanent magnet, liquid lithium, and pump duct. The electrical conductivity of the permanent magnet, which was comparable to that of the pump duct, was 29% that of the liquid lithium. Therefore, the current, which is not negligible when the permanent magnet is attached to the pump duct, leaked to the permanent magnet. The permanent magnet was insulated from the pump duct using an insulation material such as Teflon to minimize current loss, as shown in Fig. 1. The current density of the liquid lithium when the permanent magnet was isolated from the pump
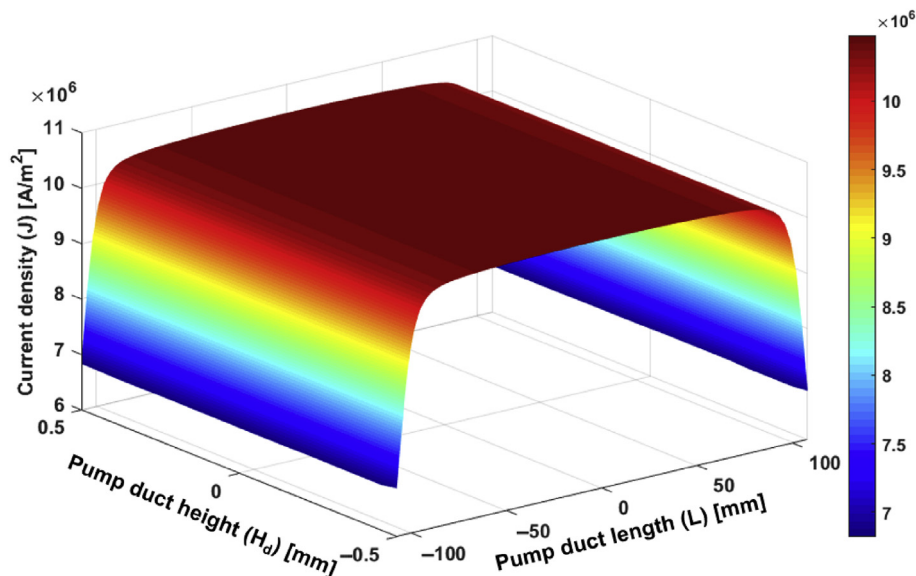

Fig. 5. Three-dimensional current density distribution at the midpoint of the pump duct width.

duct displayed a maximum value at the center of the flow, as shown in Fig. 5. The influence of the current density on the magnetic flux density was small owing to the low velocity of liquid lithium. The shape of the current density shown in Fig. 5 did not follow that of the magnetic flux density shown in Fig. 4 because the vector product of the velocity and magnetic flux density affected the current, as expressed in Equation (26).

As the length of the pump duct increased, the EMF and hydraulic loss, which disturbed the developed pressure in the DC electromagnetic pump, also increased, as indicated in Equation (34). Therefore, the duct length should be minimized to reduce the pressure loss in the pump. Fig. 6 shows the calculated permissible current I_p from Equation (35) according to the length of the pump duct, which had a fixed height of 1 mm, to increase the Lorentz force. The length of the pump duct was minimized to limit the increase in the temperature of the electrode stub to a maximum of 200°C. Accordingly, the length was determined as 216 mm to obtain a current 3740 A required for generating a pressure of 1.5 MPa.

3.3. Force density

The force density was obtained as the vector product of the current and magnetic flux densities, as expressed by Equation (28). The vector product of the x-direction component of the current density and y-directional component of the magnetic flux density was negligible, showing only 0.0013% of the total force. The contribution to the force generation by the y-direction component
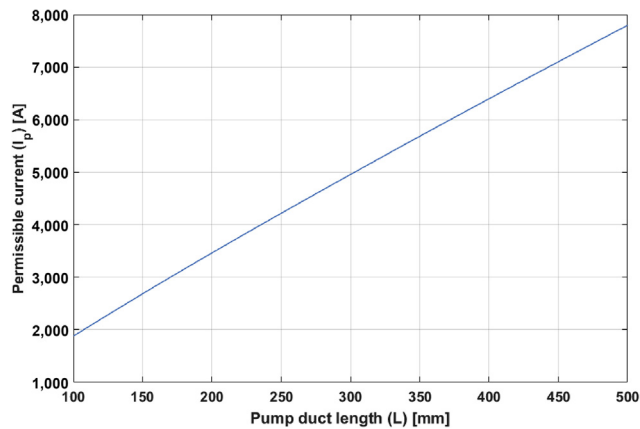
of the current density and by the x-direction component of the magnetic flux density, which were dominant in generating the electromagnetic force, is shown in Fig. 7. The magnetic flux density had negative values at the duct ends, as shown in Fig. 2. Hence, the force density also showed a 0.2% negative value at the end of the pump duct compared with the positive value in the pump duct region shown in Fig. 8. As a result, the developed pressure because of the Lorentz force was 1.617 MPa, as obtained from Equation (30). The force density due to the EMF was calculated using Equation (29) in which the velocity in the narrow channel was assumed constant and proportional to the square of the magnetic flux density, as shown in Fig. 9 [20]. The force density from the EMF, which was generated against the pumping force of the Lorentz force, is shown in Fig. 10, displaying a pressure drop of 0.117 MPa when the input current was 3740 A, which was 7.2% that of the Lorentz force. The hydraulic pressure drop obtained from Equation (32) at the narrow channel was negligible, showing 0.00026 MPa, which could be ignored compared with the electromagnetic force generated from the Lorentz force, resulting in a small contribution to the distribution of force density.

The height of the electromagnetic pump was reduced to 1 mm to increase the pump total pressure with satisfactory mechanical strength, and the width was set to 22 mm to maximize the magnetic flux density at the pump duct through the permanent magnet. The pump length was determined to minimize the hydraulic loss in

Fig. 6. Permissible current with changing pump duct length.

Fig. 8. Linear force density distribution from the Lorentz force at the midpoints of the pump duct height and width.
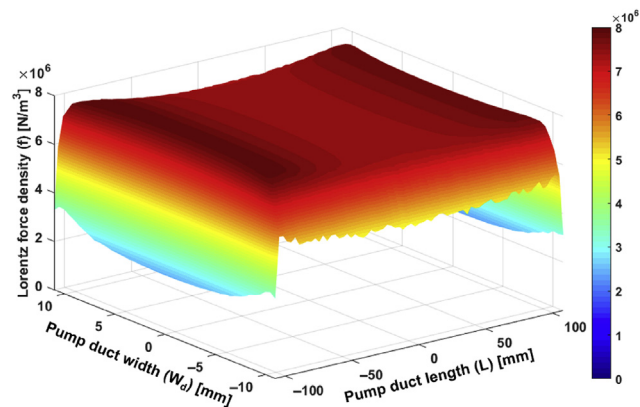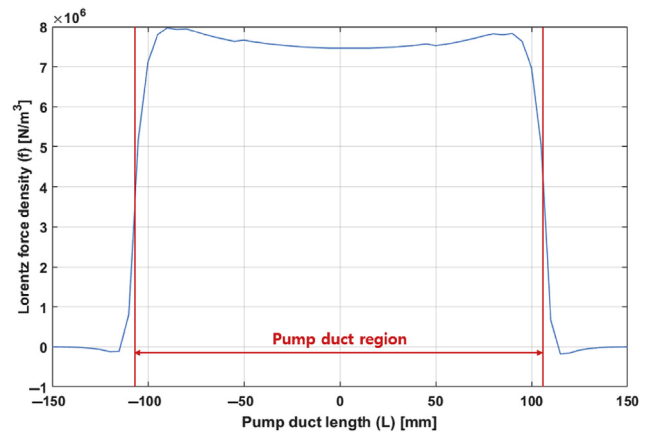

Fig. 7. Three-dimensional force density distribution from the Lorentz force at the midpoint of the pump duct height.
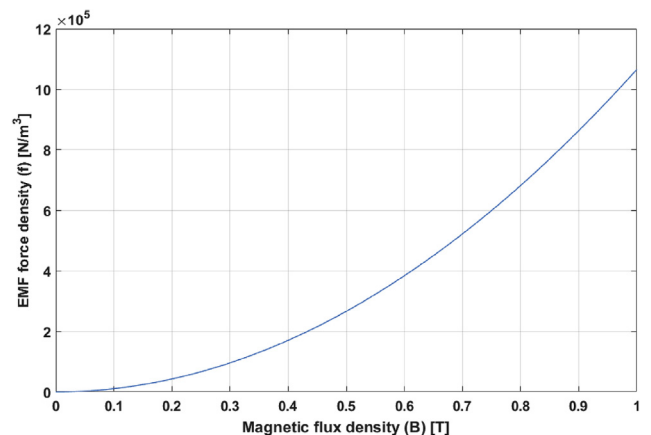

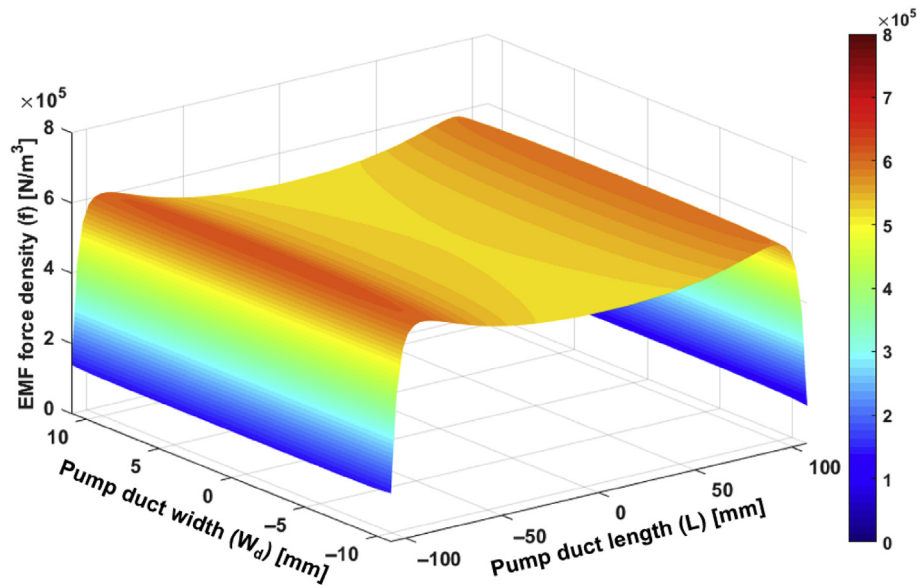Fig. 9. EMF density with the change in magnetic flux density. EMF, electromotive force.

Fig. 10. Three-dimensional force density distribution from the EMF at the midpoint of the pump duct height. EMF, electromotive force.
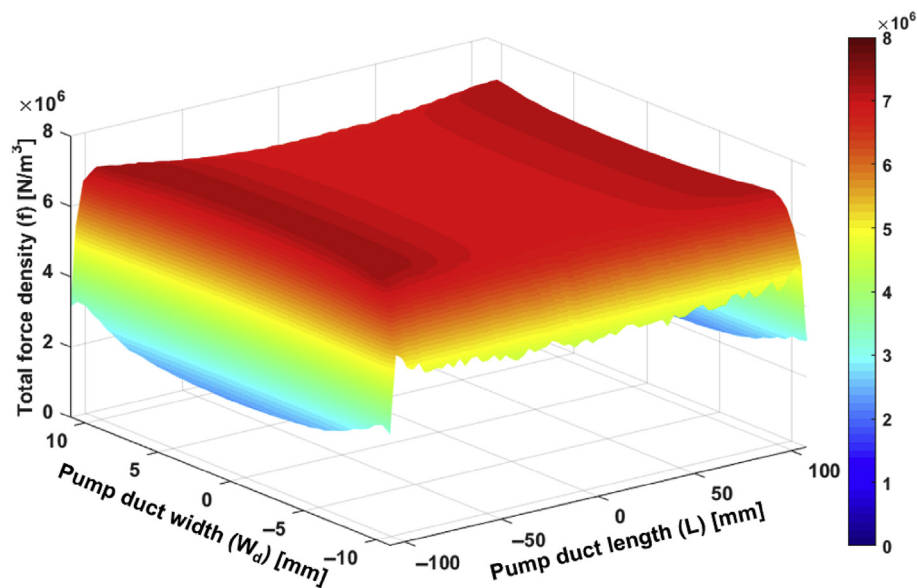

Fig. 11. Three-dimensional total force density distribution at the midpoint of pump duct height.

the flow channel by considering the permissible current. The design specifications of the DC electromagnetic pump are listed in Table 1. The developed pressure was obtained by subtracting the EMF from the Lorentz force, as shown in Fig. 11. The force density at the end of the pump duct was maximized because of the dominant Lorentz force generation at this location, which led to a developed pressure of 1.5 MPa in the DC electromagnetic pump and satisfied the 6-cm³/s flow rate requirement under an operating temperature of 200°C for the electromagnetic pump.

4. Conclusion

The force density of a DC electromagnetic pump used to create liquid lithium thin films for charge stripping of uranium heavy ions was analyzed based on the distributions of the magnetic flux and current densities. The magnetic flux and current densities were

maximized at the center part of the pump duct, whereas the magnetic flux density was minimized at the magnet edge. Accordingly, the force at both duct ends tended to appear in the opposite direction, which could disturb the normal directional flow of the liquid lithium. The electromagnetic force from the Lorentz force was 1.617 MPa, where the pressure drop of 0.117 MPa due to the EMF and hydraulic pressure drop of 0.00026 MPa were negligible. Therefore, we conclude that the geometrical and electrical parameters of the DC pump have been optimized to satisfy the requirements of a developed pressure of 1.5 MPa and flow rate of 6 cm³/s under an operating temperature of 200°C.

Conflict of interest

There is no conflict of interest.

Acknowledgments

Nomenclature

B	Magnetic flux density [T]
B_e	Magnetic flux density from permanent magnet [T]
B_i	Magnetic flux density from electrode stub [T]
B_t	Total magnetic flux density [T]
E	Electric field [kg·m/(s^3·A)]
E_t	Total electric field [kg·m/(s^3·A)]
f	Force density [N/m^3]
f_d	Darcy friction factor
H_d	Pump duct height, excluding the wall thickness along the permanent magnet direction [m]
I_p	Permissible current of the electrode stub [A]
J	Current density [A/m^2]
J_t	Total current density [A/m^2]
K	Condition coefficient of the Melson and Both equation
L	Pump duct length [m]
p	Total developed pressure of pump duct [Pa]
p_e	Perimeter of electrode stub [cm]
p_h	Hydraulic pressure loss in the pump [Pa]
Re	Reynolds number
S	Cross section of electrode stub [cm^2]
T	Permissible temperature of electrode stub [K]
T_n	Ambient temperature of electrode stub [K]
t	Time [s]
v	Velocity of the fluid [m/s]
W_d	Pump duct width, excluding the wall thickness along the electrode stub direction [m]
α	Temperature coefficient of the copper resistivity [m]
ε_0	Permittivity of vacuum [F/m]
μ_0	Permeability of vacuum [H/m]
ρ	Density of the liquid lithium [kg/m^3]
ρ'	Resistivity of the liquid lithium [Ω·m]
σ	Liquid lithium conductivity [1/(Ω·m)]

References

[1] A.U. Gutierrez, C.E. Heckathorn, Electromagnetic Pumps for Liquid Metals, Naval Postgraduate School, California, 1965.

[2] D. Kim, J. Hong, T. Lee, Design of DC conduction pump for PGSFR active decay heat removal system, in: Transactions of the Korean Nuclear Society Spring Meeting, Korea, 2014.

[3] F. Marti, P. Guetschow, Y. Momozaki, J.A. Nolen, Development of a liquid lithium charge stripper for FRIB, in: Proceedings of HIAT2015, Japan, 2015.

[4] L.R. Blake, Conduction and induction pumps for liquid metals, Proc. IEE Part A Power Eng. 104 (13) (1957) 49–67.

[5] C. Wagner, Theoretical analysis of the current density distribution in electrolytic cells, J. Electrochem. Soc. 98 (3) (1951) 116–128.

[6] T. Oka, N. Kawasaki, S. Fukui, J. Ogawa, T. Sato, T. Terasawa, Y. Itoh, R. Yabuno, Magnetic field distribution of permanent magnet magnetized by static magnetic field generated by HTS bulk magnet, IEEE Trans. Appl. Supercond. 22 (3) (2012) 9502304.

[7] M. Hughes, K.A. Pericleous, M. Cross, The numerical modelling of DC electromagnetic pump and brake flow, Appl. Math. Model. 19 (12) (1995) 713–723.

[8] R.S. Baker, M.J. Tessier, Handbook of Electromagnetic Pump Technology, Elsevier, New York, 1987.

[9] G.H. Lee, H.R. Kim, Numerical investigation and comparison of the rectangular, cylindrical, and helical-type DC electromagnetic pumps, Magnetohydrodynamics 53 (2) (2017) 429–438.

[10] D.A. Watt, The design of electromagnetic pumps for liquid metals, Proc. IEE Part A Power Eng. 106 (26) (1959) 94–103.

[11] B.K. Nashine, S.K. Dash, K. Gurumurthy, G. Vaidyanathan, Design and testing of DC conduction pump for sodium cooled fast reactor, in: 14th International Conference on Nuclear Engineering, American Society of Mechanical Engineers, 2006.

[12] N. Bennecib, S. Drid, R. Abdessemed, Numerical investigation of flow in a new DC pump MHD, J. Appl. Fluid Mech. 2 (2) (2009) 23–28.

[13] R. W, Ohse Handbook of Thermodynamic and Transport Properties of Alkali Metals, Blackwell Scientific, Oxford, 1985.

[14] B.K. Nashine, S.K. Dash, K. Gurumurthy, U. Kale, V.D. Sharma, R. Prabhaker, M. Rajan, G. Vaidyanathan, Performance testing of indigenously developed DC conduction pump for sodium cooled fast reactor, Indian J. Eng. Mater. Sci. 14 (2007) 209–214.

[15] Crane Co. (US), Flow of Fluids Through Valves, Fittings, and Pipe, Crane Co., Technical Paper No. 410, Chicago (IL), 1977.

[16] N. Takorabet, Computation of force density inside the channel of an electromagnetic pump by Hermite projection, IEEE Trans. Magn. 42 (3) (2006) 430–433.

[17] G. Xiao-Fan, Y. Yong, Z. Xiao-Jing, Analytic expression of magnetic field distribution of rectangular permanent magnets, Appl. Math. Mech. 25 (3) (2004) 297–306.

[18] A. Thess, E.V. Votyakov, Y. Kolesnikov, Lorentz force velocimetry, Phys. Rev. Lett. 96 (16) (2006) 164501.

[19] C.Y. Ho, T.K. Chu, Electrical Resistivity and Thermal Conductivity of Nine Selected AISI Stainless Steels, CINDAS Report 45, Washington, 1977.

[20] A. Thess, E. Votyakov, B. Knaepen, O. Zikanov, Theory of the Lorentz force flowmeter, New J. Phys. 9 (8) (2007) 299.